ELSEVIER

Surface Science 328 (1995) 32–46

surface science

Surface alloying and pinhole formation in ultra-thin Fe/Cu(100) films

J. Shen [a,*], J. Giergiel [a], A.K. Schmid [b], J. Kirschner [a]

[a] *Max-Planck-Institut für Mikrostrukturphysik, Weinberg 2, 06120, Halle / Saale, Germany*
[b] *Fritz-Haber-Institut / OF, Faradayweg 4–6, 14195 Berlin, Germany*

Received 1 August 1994; accepted for publication 10 January 1995

Abstract

Relatively mild annealing sometimes produces unexpectedly large changes in surface composition of ultra-thin films. We report results of a scanning tunnelling microscopy study of such annealing in an Fe/Cu(100) system. Copper appears in the surface region after a short 490 K anneal. We specifically exclude the possibility of bulk interdiffusion and conclude that this surface copper comes from the substrate through microscopic pinholes. Our primary finding is that the balance of surface free energies which strongly prefers Cu/Fe/Cu over Fe/Cu is the main driving force for pinhole formation and copper segregation. Furthermore, we report a significant surface alloying in this otherwise almost immiscible system.

Keywords: Iron; Scanning tunneling microscopy; Surface diffusion

1. Introduction

The Fe/Cu(100) ultra-thin film system is often called a benchmark system for metal-on-metal epitaxy as well as for magnetic investigations. The system was predicted [1] and found [2–7] to have striking magnetic properties due to the reduced dimensionality. The structure of this system has also been extensively studied [8–10], since very thin iron films on Cu(100) substrates grow pseudomorphically in a slightly distorted fcc-Fe structure [11,12], which does not exist in bulk below 928°C [13]. The growth mode is found to be very complicated; it depends very much on kinetic limitations and is strongly affected by the inherent instability of this fcc-phase [9]. This is sometimes utilized to achieve better film quality; for example: low temperature deposition followed by annealing has been suggested as the best way to make monoatomically smooth films [8]. The film morphology has proven to be a very important factor in determining the magnetic properties of this system from variant results obtained by different groups using slightly different preparation conditions [3,14–16].

Studying the annealing effects in this ultra-thin film system is not only important for improving the thin films' morphology, but also is important for some magnetic measurements such as Curie temperature, because in some measurements fairly high temperature is used and it is likely to cause a rearrangement of the overlayer. In contrast to the enormous amount of work on magnetic and structural properties of Fe/Cu(100) ultra-thin film, the annealing

* Corresponding author. E-mail: shen@secundus.mpi-msp.halle.mpg.de.

SSDI 0039-6028(95)00024-0

effects have not yet been thoroughly investigated. Previous work on thin film systems, e.g. Fe/Au(100) [17], Au/Ag(111) [18], Ni/Cu/Ni(100) sandwiches [19], Rh/Ag(100) [20], Co/Cu(100) [21] and Fe/Cu(100) [22] found that by annealing the films, not only the surfaces of the films were smoothed, but also the top one or two layers were found to be rich in substrate material. These processes called segregation were observed to occur rapidly at surprisingly low temperatures. Recent STM work [23] presented clear evidence that during annealing of another ultra-thin film system Co/Cu(100), microscopic pinholes grow deep into the substrate as Cu migrates to the top of the film by diffusing along the bottom and the walls of these pinholes. Thus it is very interesting to know if similar phenomena also appear in other thin film systems like Fe/Cu(100), and, more importantly, what physical mechanism drives this process.

The aim of this paper is to study the effects of annealing on morphology and composition of Fe/Cu(100) films. The results of a scanning tunnelling microscopy (STM) and Auger electron spectroscopy (AES) study of annealing process are presented in detail. The film surface was found to be copper-rich after annealing, and the transport mechanism and main driving force for this phenomenon are clearly shown. Furthermore, strong evidence will be presented for surface alloying at elevated temperatures.

2. Experimental procedure

The substrate was initially prepared by 2–5 h room temperature sputtering (500 eV) until the C(273)/Cu(60) Auger ratio was less than 5%, followed by 10 min sputtering (300 eV) at 815 K. After several cycles of this procedure, we routinely obtain surfaces with several hundred nanometers large and atomically flat terraces. The cylindrical mirror analyser (CMA) based AES showed that the copper sample was Auger clean (< 0.1 at% for most elements). Fe was sublimated from a wire of 99.999% purity heated by electron bombardment to yield deposition at 0.05–0.2 ML/min, with the maximum pressure rise typically limited to 8×10^{-9} Pa (worst case 3×10^{-8} Pa). The iron vapour beam intercepts the sample at a small angle (15° to surface plane). On the macroscopic scale the deposited film was uniform as judged by the Auger ratios, though, on

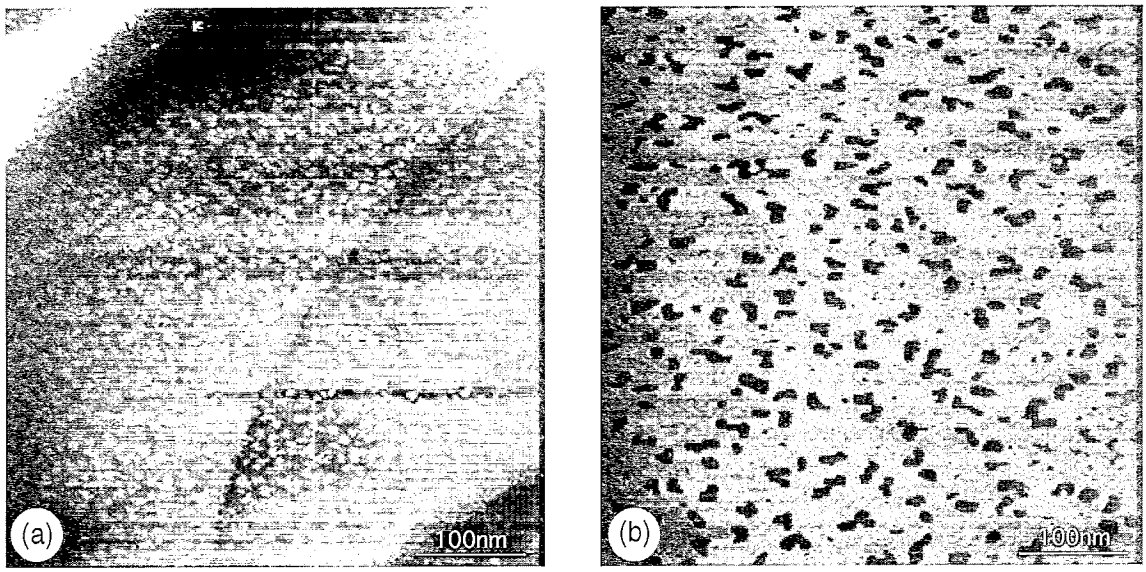

Fig. 1. STM image of 2.5 ML room temperature deposited Fe/Cu(100) film. Scanning area is 500×500 nm^2. $V_{bias} = 0.6$ V, $I_t = 0.6$ nA. (a) Before annealing; (b) after annealing at 490 K, 10 min. Note in the left image a catenary step band system characteristic of a well prepared Cu substrate and the distribution of Fe islands. Dark areas in the right image are openings into the copper substrate from which copper flows out to cover the surface.

the microscopic level, STM images clearly showed significant shadowing next to large protrusions which are often associated with big step-pinning clusters [24].

The growth of Fe thin films on copper was observed by the in-situ, custom-designed STM [25]. The experimental set-up allows us to follow the same area after each step of Fe deposition, which provides an accurate way to count the film thickness [26]. The Fe films were first deposited in the STM stage at room temperature (300 ± 5 K), then transferred to a manipulator for annealing and for Auger electron spectroscopy. The annealing temperature was manually controlled and measured by a K-type thermocouple attached directly to the sample. In order to study the complete history of the development of individual structural features in the film, we usually retrieve the same region of the sample surface in the STM after annealing.

STM images were taken in the constant current mode, with positive sample bias 0.6–1 V and tunnelling current 0.1–0.3 nA. The scanning line rate was 0.1–2 Hz depending primarily on the scanning size and the morphology of the area. From time to time the scanning parameters were varied to check for any tunnelling induced artifacts in acquired images, and none were found for the original Cu and as-grown Fe surface. However, a significant dependence on sample bias was found after annealing to temperatures sufficiently high to create pinholes and to diffuse Cu to the surface.

3. Results

In this section, the results are presented in three separate parts: (1) coverage dependence of pinhole formation, (2) formation of Fe–Cu surface alloy on the annealed films, and (3) driving mechanism for copper segregation. The discussions of the results will be given in the next section.

3.1. Coverage dependence of pinhole formation

Fig. 1 shows the constant current topography image of a 2.5 ML iron film before and after annealing. Fig. 1a is a 500×500 nm^2 area view of the 2.5 ML Fe film as deposited at room temperature. The surface is almost fully closed by the 2nd Fe layer and the 3rd uncompleted layer is seen as irregularly shaped small islands. Large scale structures in the image are terrace steps forming a catenary step band

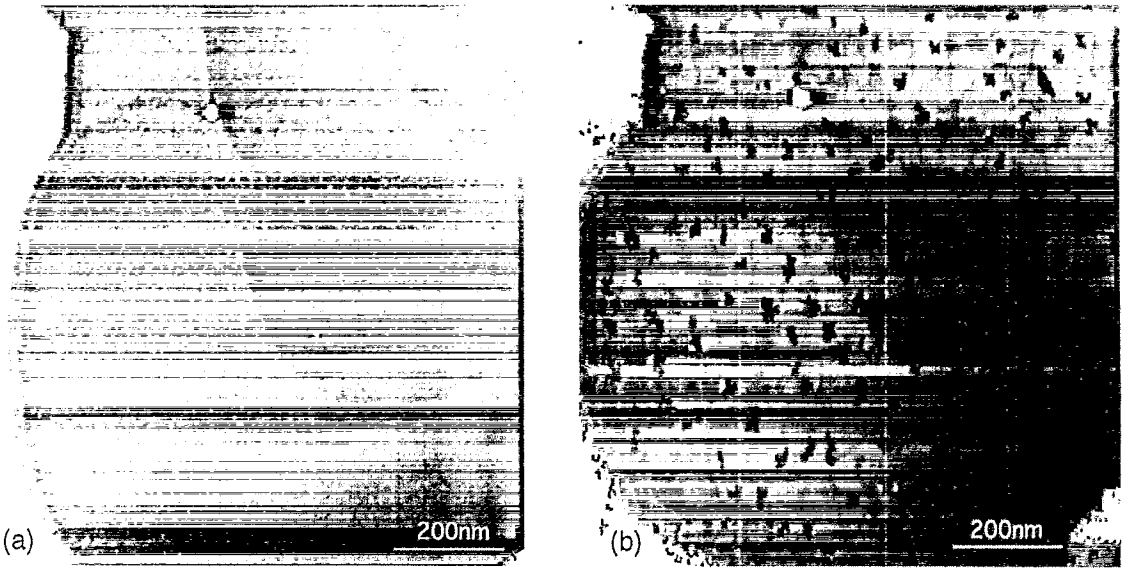

Fig. 2. STM image of 3 ML room temperature deposited Fe/Cu(100) film. Scanning area is 1000×1000 nm^2. (a) Before annealing, $V_{bias} = 1$ V, $I_t = 110$ pA; (b) after annealing at 490 K, 10 min, $V_{bias} = 1$ V, $I_t = 135$ pA. Note the much lower number density of pinholes generated during annealing in this 3 ML film as compared to that of 2.5 ML thick (previous image).

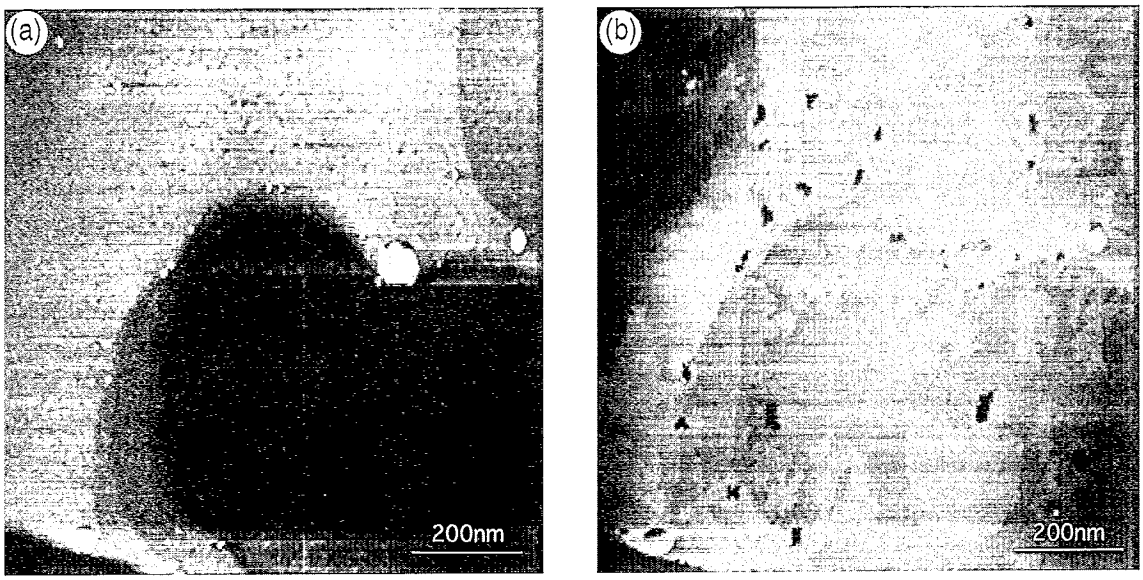

Fig. 3. STM image of 4 ML room temperature deposited Fe/Cu(100) film. Scanning area is 1000×1000 nm^2. (a) Before annealing, $V_{bias} = 1$ V, $I_t = 110$ pA; (b) after annealing at 490 K, 10 min, $V_{bias} = 900$ mV, $I_t = 110$ pA. Most of the pinholes are now visible only around step band edges and surface imperfections. Note the characteristic structures that are associated with each pinhole. These are the only bias dependent features seen on this sample and are, therefore, interpreted as the extent to which copper can diffuse out of the pinholes under given annealing conditions.

system typical of well prepared metallic surfaces [24]. Annealing this film at 490 K for 10 min results in a much different topography – see Fig. 1b (not the same area as before annealing). Immediately apparent from the STM image are dark patches. These are pinholes extending well below the original Cu sur-

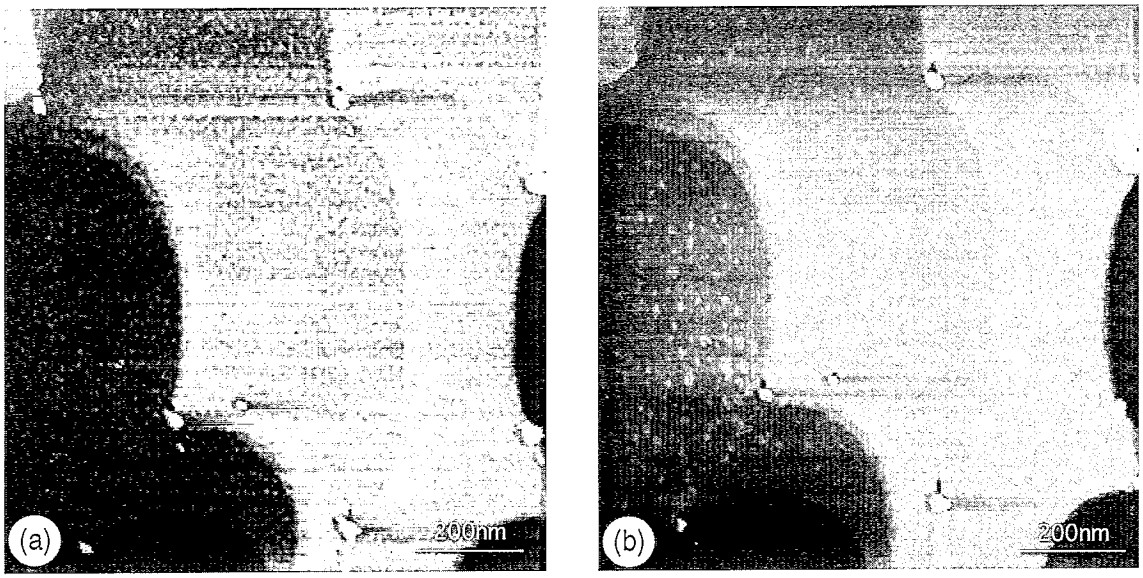

Fig. 4. STM image of 5 ML room temperature deposited Fe/Cu(100) film. Scanning area is 1000×1000 nm^2. $V_{bias} = 900$ mV, $I_t = 110$ pA. (a) Before annealing; (b) after annealing at 490 K, 10 min. Note that only a few pinholes appeared on the surface of this relatively thick film and none of them was nucleated on atomically flat parts of the surface.

face. They are seemingly randomly distributed on the surface with the average density of 1330 μm^{-2}. The surface between these pinholes appears corrugated but otherwise the whole 500×500 nm^2 area is quite homogeneous. The corrugation is bias dependent and has an amplitude well below that of the Fe interplanar distance. It is important to note here that no such bias dependent corrugation was ever seen by us in any room temperature deposited Fe films. We will discuss this corrugation later in this paper.

Similar pinhole formation is also observed in thicker films. These are shown in Figs. 2–4 for 3, 4 and 5 ML thick films, respectively. Note that in all three cases the images before and after (10 min, 490 K) annealing were taken on the same area of the sample in 1000×1000 nm^2 size.

Increased thickness results in the drastic reduction of the number density of pinholes generated in these films. The density of pinholes decreases from 1330 μm^{-2} for 2.5 ML film down to 7 μm^{-2} for 5 ML. Apparently, with increasing thickness it becomes harder to nucleate channels to the copper substrate. For example, in the case of the 5 ML film (Fig. 4) only several pinholes are present and they exist only in the vicinity of step band edges or large contamination clusters where shadowing may cause the Fe film to be locally thinner. For the 4 ML (Fig. 3) film there are still several pinholes nucleated on atomically smooth areas. The immediate conclusion is that the 4 or 5 ML film is thick enough to preclude pinhole generation on atomically smooth areas. The limiting density simply reflects the quality of the surface, as the only pinholes observed in thick Fe films are generated in the vicinity of the surface imperfections.

Another effect of annealing that can be deduced from Fig. 2 and Fig. 3 is the appearance of the additional material on top of the film. For example, there are three layers seen in Fig. 2 before annealing, the 2nd, 3rd and the 4th which together amount to the total coverage of 3 ML. After annealing there are only the 3rd and the 4th layer islands in the topmost layer and the total coverage is 3.7 ML. Similar histogram calculations for 4 ML thick film show 0.4 ML of additional 5th layer islands appearing after annealing on top of the surface. These additional islands distribute uniformly on the surface of 3 ML films, but in the 4 ML annealed film they are rather

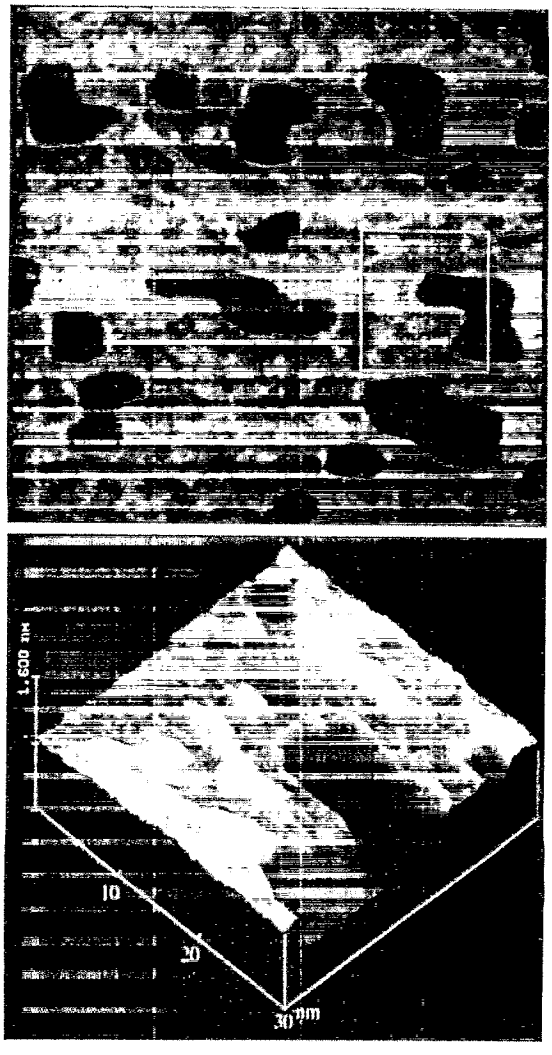

Fig. 5. 120×108 nm^2 image of the 2.5 ML annealed film. Perspective view of the box area is shown below. Each pinhole is surrounded by a corrugated surface phase seen in the image as light patches. The apparent amplitude is much less than a monolayer step and it varies with tunnelling parameters. The lower panel shows a typical pinhole with characteristic straight edges along the [011] directions.

localized around the pinholes. We calculated the volume of the pinholes, and found that they are quite close to the volume of the additional islands in both 3 and 4 ML annealed films.

The top view, higher magnification images of the 2.5 and 3 ML annealed films are shown in Figs. 5 and 6, respectively. The scale of these images nicely accentuates the corrugated phase that exists around these pinholes. Figs. 5 and 6 also show perspective

views of typical pinholes. They clearly indicate that these pinholes are not really "holes", but more like several nanometers deep flat depressions with an average lateral dimension in the range of some tens of nanometers. Anyhow, we will keep the term "pinhole" for the rest of the paper but the reader should keep in mind their actual dimensions. It is interesting to note that the pinholes show clear crystallographic preferences, their edges tend to be oriented along the [011] and [0$\bar{1}$1] directions. In the 2.5 ML film, the actual sources of copper are smaller holes inside the irregularly shaped larger holes; these small holes are deeper than the substrate and their edges are still close to the [011] and [0$\bar{1}$1] direction (Fig. 5). The wall steepness is estimated to be close to 50°–60° off the surface normal. As the (111) face is 55° off the surface normal and has the lowest energy in fcc crystals, it is quite possible that the holes' walls are (111) facets.

Not immediately apparent in Figs. 1–4 is another trend: with increasing film thickness, the depth of pinholes increases much faster than the increased film thickness. For example, the average depth of pinholes for 2.5 ML film is around 0.8 nm, but the average depth for 3 ML film is 2.1 nm. They also become somewhat larger in diameter – starting with the average of 127 nm^2 on 2.5 ML film and become some 350–500 nm^2 on thicker films. These findings are summarized in Table 1 and will be discussed later in the paper.

In addition to changes in the morphology, annealing results in changes in the composition of the film. This is illustrated in Fig. 7 which shows the ratio of Fe(47) and Cu(60) Auger peak amplitudes as a function of annealing time for 2.5, 3 and 4 ML thick films. In all three cases, the Cu(60)/Fe(47) ratio slightly goes down at annealing time 100–200 s, then rapidly goes up at 200–350 s, and finally goes into the saturation.

3.2. Formation of an Fe–Cu surface "alloy" on the annealed films

We now return to the bias-dependent corrugated phase seen in images of annealed films. Fig. 8 shows the characteristic feature of the corrugated phase, with STM top view images on the left and the corresponding height histogram of each indicated area on the right. The upper left image is the 100 × 100 nm^2 top view of a 3.1 ML annealed film. The corrugated phase seems to have a tendency to concentrate around step and island edges. The height distribution of surface features is shown in the upper histogram. The highest peak (1) represents the darkest area in the image, peak 2 represents the corrugation associated with the darkest area level, peak 3 represents the 4th layer islands and peak 4 represents the corrugation on those islands. At a sample positive 900 mV bias voltage, the amplitude of the corrugation is around 0.7 Å, but this changes with

Table 1
Coverage dependence of annealing effects at 490 K for 10 min

Coverage (ML)	Pinhole density (μm^{-2})	Pinhole average size (nm^2)	Pinhole average depth (nm)	General description of annealing effect
0.3	–	–	–	Island size becomes larger, bias-dependent fractional-step-height features appear both on substrate and islands
2.5	1328	127	0.8 ± 0.2	Pinholes and bias-dependent fractional-step-height features appear uniformly on whole surface
3	164	375	2.1 ± 0.1	Pinholes and bias-dependent fractional-step-height features appear uniformly on whole surface
4	38	515	4.0 ± 0.7	Pinholes were mostly formed around large clusters or step bands, fractional step height features show the tendency to concentrate around the pinholes
5	7	42	1.8 ± 0.5	Pre-existing holes (due to the shadowing) become deeper; fractional-step-height features are localized around these holes. No new pinholes formed

the bias voltage especially when the polarity is reversed. The lower left image shows the same area as in the upper left one, but with one additional monolayer Fe deposited on the top. Its histogram data clearly show that there are almost no fractional-step-height corrugation but only monolayer height islands. Note that additional Fe grows on this annealed 3.1 ML Fe film surface with a high nucleation density.

Fig. 9 shows that these corrugations are strongly bias dependent. Fig. 9a was taken at 900 mV (sample positive), the average height of the corrugations is around 0.7 Å. Fig. 9b was taken at −900 mV, and the average height is only 0.2 Å.

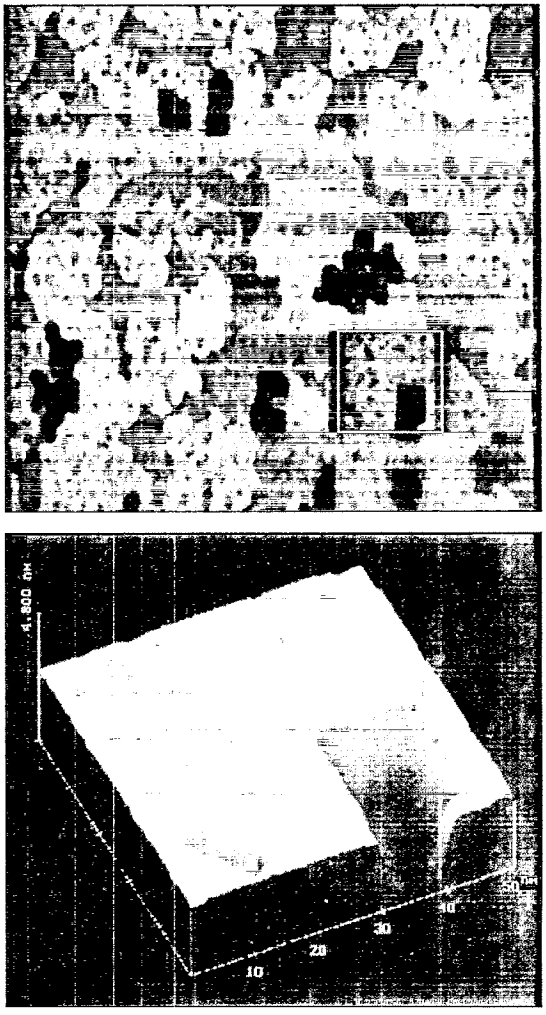

Fig. 6. 300×277 nm^2 image of the 3 ML annealed film. Perspective view of the box area is shown below. Two monoatomic levels are seen in this image that of the 3rd and 4th layer. All of them show significant and homogeneous corrugation.

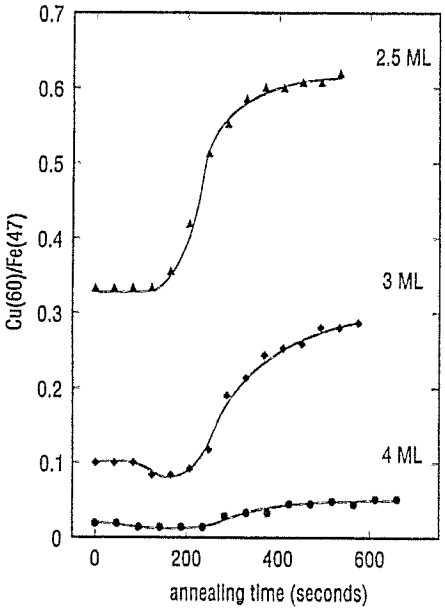

Fig. 7. Plot of Auger Cu(60)/Fe(47) ratio versus annealing time at 490 K in 2.5, 3 and 4 ML Fe/Cu(100) film, respectively. The solid lines are only for guiding the eyes.

The evolution of the annealing process is demonstrated in Fig. 10. Fig. 10a is the 300 × 300 nm^2 top view image of a 3.5 ML Fe film before annealing; the screw dislocation (its pinning point is marked by the white circle) in the bottom part of the image is used as a registration mark. Fig. 10b is the same area after 2 min of annealing. The height profile along the indicated white line is shown below in Fig. 10d. The profile demonstrates the relative height of various surface structures: pinholes (marked as 3), monosteps (marked as 1 and 2) and fractional-step-height corrugation, etc. Fig. 10c shows the morphology of this area after another 5 min annealing. Apparently annealing results in coalescence of the islands and the appearance of corrugation with fractional-step-height relative to the dark area. The corrugated areas concentrate around pinholes and island edges – Fig. 10b. Further annealing causes more corrugation to appear on the surface, and the whole area becomes more uniform – Fig. 10c.

In Fig. 11 we show the annealing effect during initial stages of RT grown Fe film. Figs. 11a and 11b show the same 1 × 1 μm^2 area topview images of

0.3 ML Fe film before and after annealing, respectively. The regions indicated by the white borders are shown in larger magnification in Figs. 11c and 11d. At room temperature the Fe film grows in a high nucleation density in the initial stages, as indicated by Fig. 11c. No bias or tip dependent features has been found in this image. But after annealing this 0.3 ML film, small corrugations which are bias dependent appeared on the surface. Since the height of this corrugated phase is less than 0.2 Å, we are showing them in a contrast that makes all the monolayer islands to become fully white in Fig. 11d. This also hides the existence of similar corrugation on top of the islands.

3.3. Driving mechanism

The data presented above indicate that the pinholes do not appear in thick films. It is interesting to determine if their generation in thin films can be blocked in some other way. If so, the blocking technique itself should provide an important clue to the nature of the mechanism that drives the pinhole generation in the first place. Since the final result of annealing is a Cu-rich surface, suggesting the Cu/Fe/Cu sandwich may be an energetically preferable configuration over that of Fe/Cu, we prepared such a sandwich and subjected it to the same annealing regime as before. The results of this experiment are

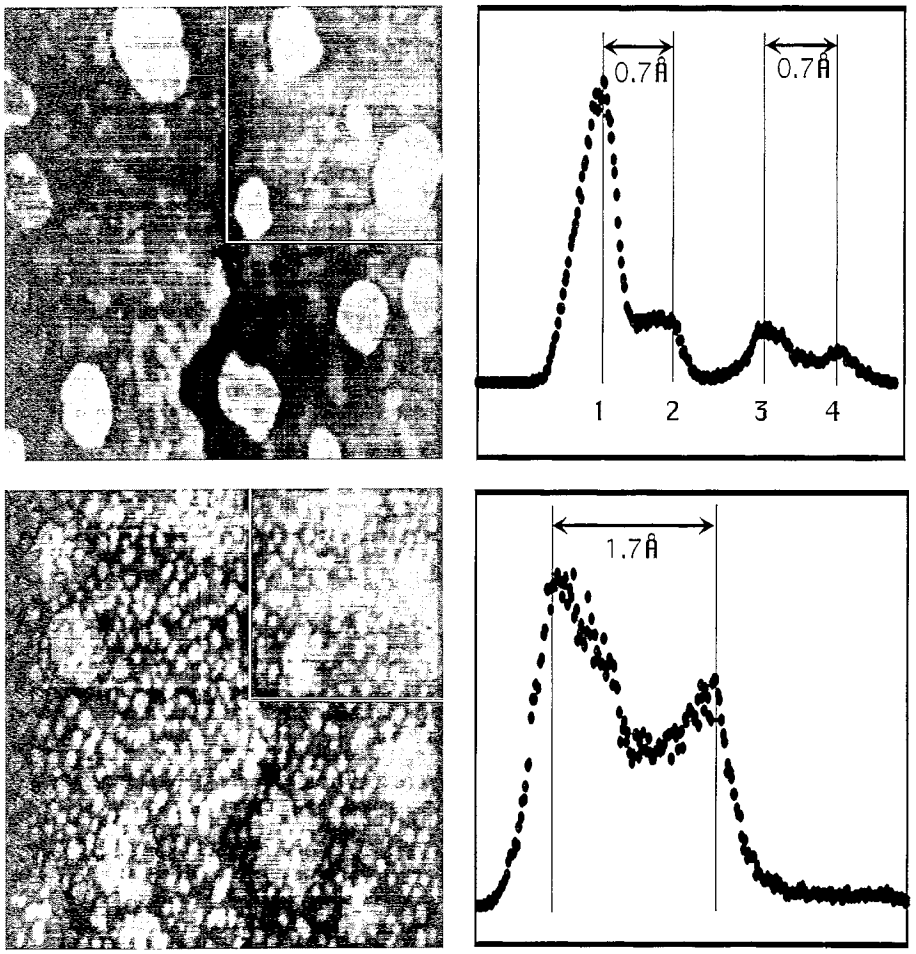

Fig. 8. The upper left image shows a 3.1 ML Fe/Cu(100) film after annealing at 440 K, 5 min. Scanning area is 100×100 nm^2. Note the surface corrugation. Upper right is the histogram of the indicated area, showing that the corrugation has the well defined amplitude of 0.7 Å. After additional 1 ML iron deposition at room temperature, the fractional-step-height features vanished. The top view is shown in lower left, and the histogram of the box area is shown in lower right.

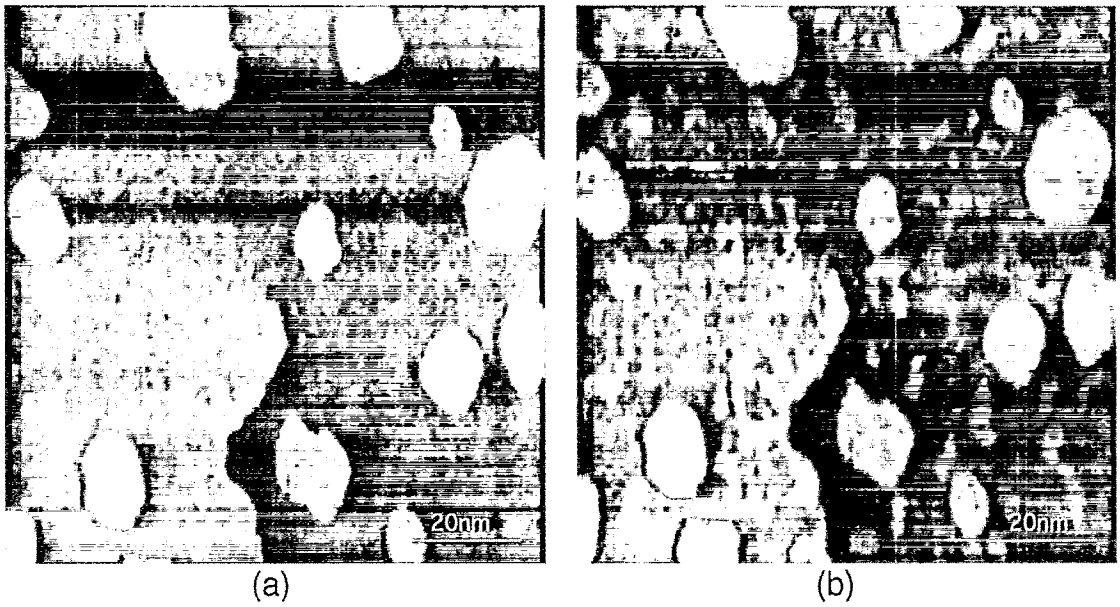

Fig. 9. The corrugations that appeared after annealing are strongly bias dependent; (a), (b) show 3.1 ML annealed fim (100×100 nm^2) in the same contrast, but at -900 and $+900$ mV, respectively. The average height of the corrugations is 0.2 Å in (a), much less than 0.7 Å in (b).

presented in Fig. 12. Panel (a) is the topview of as-grown 3.3 ML thick iron film. Panel (b) shows the topography of this area after capping it with 0.8 ML of copper. Note that copper grows partly in the same layer as the Fe 4th layer islands, and partly as the fifth layer islands. The initial stages of Cu growth on Fe are obviously not in a high nucleation density mode like that of the Fe growth on Cu. In fact, the 5th layer copper islands' size is quite comparable to that of the 4th layer Fe islands. Fig. 12c shows the topography of this Cu/Fe/Cu sandwich after the standard annealing (10 min, 490 K). The small depressions observed in areas between the white islands and the large dark patches have fractional-step depth which is bias dependent. The large dark patches are not pinholes but have a depth between 1 and 2 monolayers; this is due to the fact that the small depressions also exist in the third layer. Fig. 12d shows the height profile along the indicated white line in Fig. 12c. The depth of the large dark patch (marked 3) is almost equal to the height from the bottom of the fractional-step depression (marked as 1) to the top of the mono-step island (marked as 2). We checked all the area in our STM scanning range after annealing; no pinholes have been found in this capped film. The Fe(47)/Cu(60) Auger ratio changed very little compared with the changes seen in Fig. 7 for the uncapped Fe/Cu film.

4. Discussion

We start our discussion from the Auger data in Fig. 7. The initial Cu(60)/Fe(47) Auger ratio strongly depends on the thickness, which is 0.33 at 2.5 ML, and 0.1 at 3 ML. This change demands an inelastic mean free path to be less than 2 Å, which is much smaller than the typical values for low energy electrons (~ 4 Å at 50 eV). Some amount of Fe–Cu intermixing could be a plausible explanation. The reason why we do not observe any indication of intermixing, similar to that first observed by Chambliss and co-workers [27,30], could be that the chemical identity of our STM tip is very stable since the Fe beam covers the tip while deposition takes place. During annealing the Auger ratios change strongly indicating that the surface region becomes copper-rich. The slight depression at 100–200 s might be related to the coalescence of the islands which occurs before pinhole formation and copper segregation. The STM images shown before indicate that some copper is transferred to the top of the film

during annealing. This is consistent with the strong changes in the Auger ratios in Fig. 7. However, the probing depth in Auger experiments is such that we cannot exclude some presence of copper in the bulk of the Fe films. Thus the two relevant questions are: (a) is the additional copper present only in the topmost layer of the Fe film or is it distributed throughout the whole thickness of the film, and (b) are pinholes the only source of the additional copper or is a bulk diffusion process through the film contributing?

To address these questions we first note that there are no intermediate phases in the bulk Fe–Cu system. The solubility of Fe in Cu is negligible, while the solubility of Cu in Fe depends on its phase – it is small for α-Fe but can be as high as $\sim 8\%$ in γ-Fe [28].

As shown in Table 1, the bottom of the pinholes reaches far into the substrate. For example, in the 4 ML Fe annealed film, the average depth of the pinholes is about 40 Å. This should be compared with the thickness of the 4 ML Fe film which is only some 8 Å thick. Thus most of the material coming out of the pinholes must be substrate copper. When we calculate the total volume of pinholes directly from the data in Table 1, and if we assume that all this material stays on top of the films' surface, we should get about 0.7 and 0.4 ML additional layers in

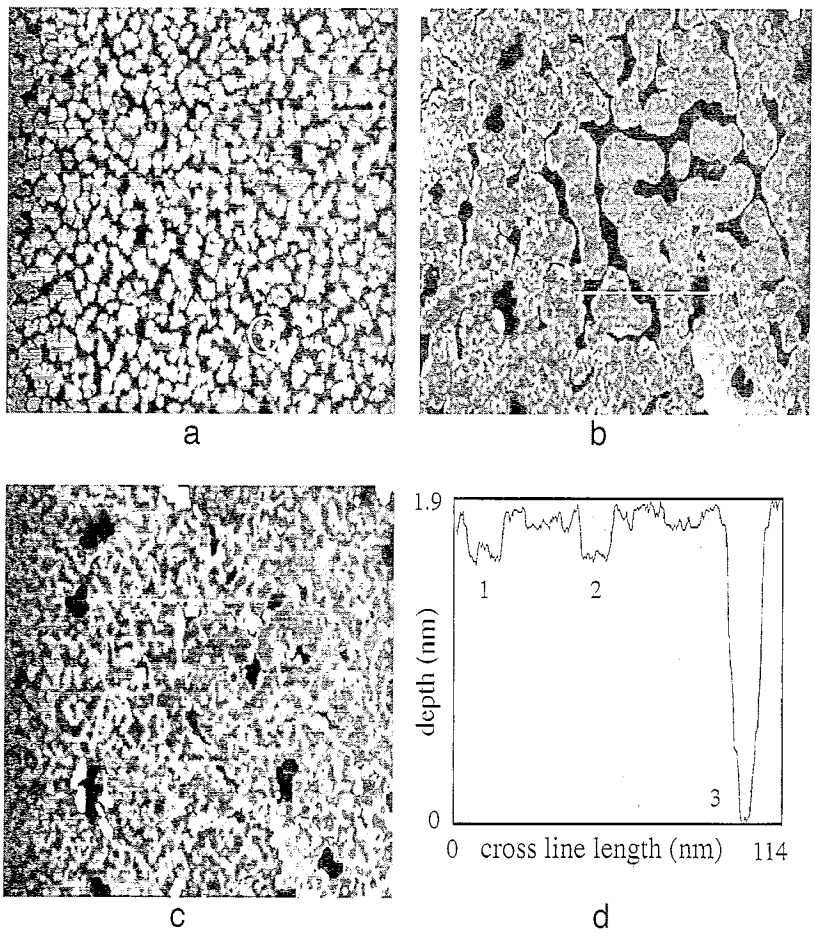

Fig. 10. STM observation of the process of surface morphology change in a 3.5 ML film during annealing at 490 K. Scanning area is: 300×300 nm^2. $V_{bias} = 900$ mV, $I_t = 110$ pA. (a) Before annealing; (b) after 2 min annealing; (c) after another 5 min annealing; (d) the profile plot of the marked line scan in (b). The profile shows the depth of mono-steps (1 and 2) and pinhole (3), the fractional-step corrugations are shown as deviations from the straight line on the line scan. Note how deep the pinhole appears relative to monolayer steps.

3 and 4 ML annealed Fe films, respectively. This is indeed consistent with the coverages of the additional islands which appear after annealing in both 3 and 4 ML Fe films. In addition, in the 4 ML annealed film (Fig. 3), the additional islands are quite localized around pinholes, showing an obvious relation to the pinholes. These observations strongly indicate that the material flowing out of the pinholes, most of which is copper, goes to the topmost layer of the film after annealing. This is further supported by Auger data which are consistent with model calculations assuming the additional copper located in the topmost layer only.

Still another but somewhat weaker evidence for copper residing on top of the surface comes from the experiment in which an additional 1 monolayer iron

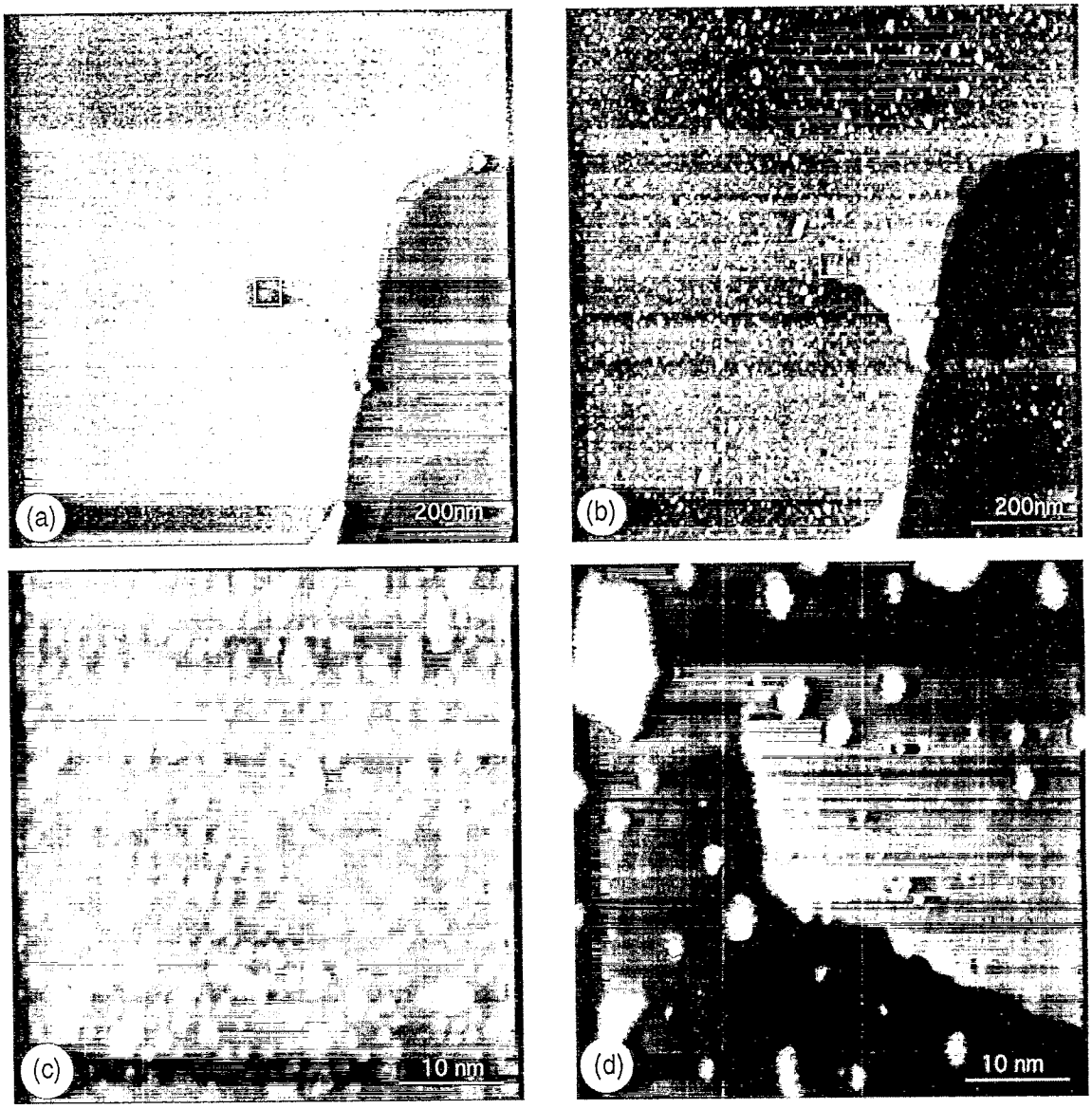

Fig. 11. Large area (1000×1000 nm^2) overview of 0.3 ML Fe/Cu(100) film (a) before and (b) after 490 K, 10 min annealing. Scanning parameters are $V_{bias} = 900$ mV, $I_t = 110$ pA; (c), (d) show the box areas (500×500 nm^2) in (a) and (b), respectively. No fractional-step corrugations can be found in (c), but these kinds of corrugations appear on the surface after annealing in (d). Note that the large bright islands in (d) are mono-step islands.

was deposited on top of an annealed 3.1 ML film (Fig. 8, lower left). This additional iron grows in a high nucleation density mode, which is characteristic of the initial growth mode of Fe on clean copper [29], thus suggesting again a copper-rich surface.

The majority of the evidence thus points to microscopic pinholes as the primary source of copper and to the conclusion that the excess copper seen in the Auger data is predominantly located in the topmost layer

The next point we want to discuss in this section is the nature of the fractional-step-height corrugated phase which appears in most of the annealed Fe films. Fig. 9 clearly shows that when the bias voltage is reversed, the height of the corrugations can be changed by as much as 0.5 Å. This is a strong indication that these corrugations must be closely related to the electronic local density of states (LDOS). The imaging contrast is seen consistently in annealed films if the bias is kept constant, with the same height observed even in different samples and for different tips. The stability of this contrast indicates that this contrast does not arise from a tip anomaly that was described in Ref. [30].

Another possibility, namely that the fractional-step-height corrugation is due to the height difference of copper and iron islands can be ruled out because all our experiments on the initial growth

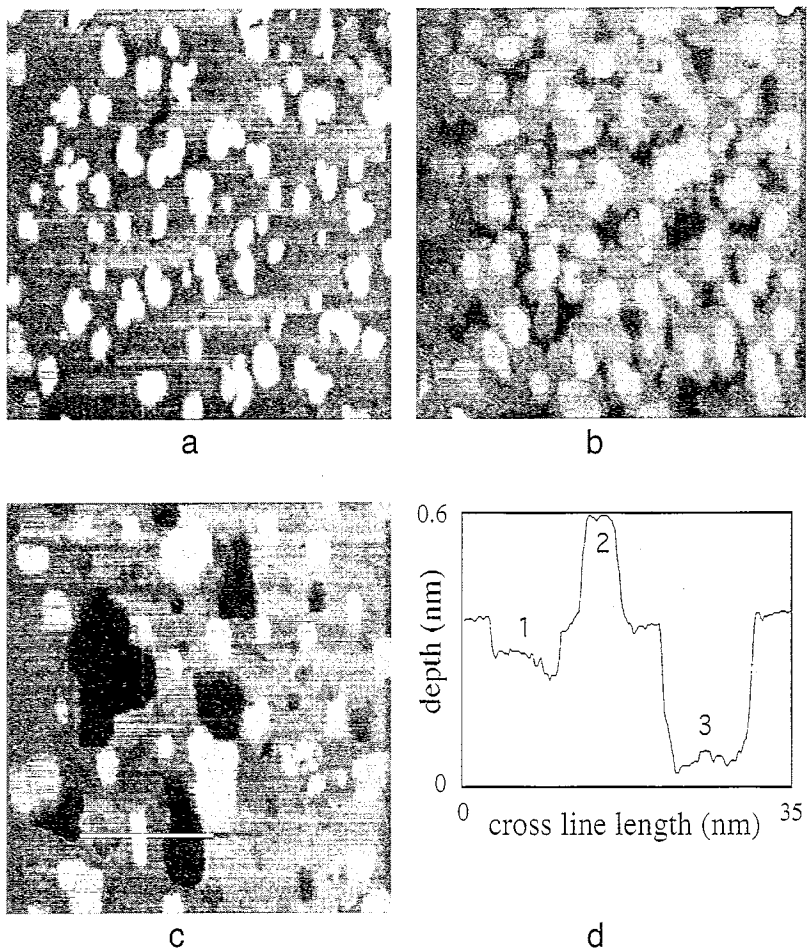

Fig. 12. (a) 3.3 ML Fe/Cu(100) film; (b) the same film but capped by 0.8 ML Cu; (c) the copper-capped iron film, after annealing at 490 K for 10 min. Scanning area is 100×100 nm^2; (d) the profile plot of the marked line scan in (c). The profile shows the relative height of the fractional-step depression (1) and mono-step island (2) and a mono-step opening of the film with fractional-step depression inside (3).

study of Fe/Cu(100) consistently show that the height difference between iron islands and a copper monostep cannot be detected with the vertical resolution of our STM [29]. Any other geometrical origin of the corrugation is unlikely because as shown in Figs. 8 and 9, the corrugation disappears almost completely when some additional Fe (even as little as one monolayer) is evaporated onto the annealed film (Fig. 8).

Having excluded the "chemically" sensitive tip or geometrical origin as a possible explanation for fractional-step-height corrugation seen in annealed films, we propose that the corrugation reflects random surface 2D alloying. As in any binary alloy one expects many small cluster units, e.g. Fe atoms surrounded totally by Cu atoms and vice versa. In fact, at a surface, the tendency for short range clustering is enhanced because of reduced coordination [33]. When isolated, such clusters show sharp "molecular" electronic levels. On the solid surface one expects some smearing out by fluctuation in random potential but some structure in the surface local density of states should remain. Somewhat surprising is that the corrugations show an average height of 0.7 Å, which is unusually large for electronic structure in metals. We note however that a similar magnitude was also observed by Mo and Himpsel [34] in the Cu/W(110) system. They report bias-dependent contrast at the step edges of W, and attribute it to a Cu-induced empty state (~ 0.6 eV above Fermi level). This interpretation is further supported by their inverse photoemission results. The reason for us to believe that the corrugations observed in the annealed Fe/Cu(100) system is due to clustering in the surface "alloy" instead of the pure Cu or pure Fe patches is that no bias dependent features have ever been found by us at the step edges of Cu decorated by Fe atoms.

Another reason to believe the corrugation reflects the presence of an inhomogeneous Fe–Cu surface alloy, comes from the results of an annealing experiment on a submonolayer Fe film (0.3 ML). It has been generally agreed that in the Fe/Cu(100) system, Fe and Cu will intermix or form a surface alloy when iron is growing at substrate temperature significantly above room temperature, and there is some evidence that at submonolayer coverages Fe–Cu intermixes at or below room temperatures [8,30]. Annealing such films should, in view of previous results, produce surface alloying. And fractional-step-height features characteristic of extensive surface alloying were indeed found in annealed 0.3 ML Fe films – Fig. 11.

A related question is: in these fractional-step-height features, what are the components of bright and dark areas? (Bright and dark refers here to colour-coding of images acquired with sample-positive bias.) The answer to this question is clearly given by Fig. 10, which shows the evolution of the annealing process. Apparently the annealing results in coalescence of the islands and the appearance of corrugation features which have fractional step heights relative to the dark area. In Fig. 10b these corrugated areas concentrate around pinholes and island edges. Further annealing causes more corrugations to appear on the surface, and the whole area becomes more uniform – Fig. 10c. The AES data show that from (b) to (c) the film surface become more Cu-rich, thus this fractional-step-height corrugation must be closely related to diffused Cu. We point out here that brighter areas are very likely Cu-rich parts of the surface – their fraction increases with annealing time. This is further supported by the following observation: in the 3 ML annealed film, the fraction of the brighter features is approximately 70%. This is consistent with 0.7 ML coverage which the materials coming out of the pinholes can form. Since most of this material is Cu, then the brighter features should represent Cu-rich patches in Fe–Cu surface alloy.

After having presented most of our experimental results, we finally come to the stage to discuss the driving mechanism for the whole process. It is not surprising that this system shows such a strong preference for surface segregation. Firstly, since the surface tension of Cu is significantly lower than that of Fe, it is favourable for Cu to segregate to the surface. This is indeed observed for fractional coverages of Fe on copper – see the 0.3 ML experiment discussed above (Fig. 11). Such a process seems to require elevated temperatures even for submonolayer coverages where it is relatively easy for Fe adatoms to be incorporated into the Cu substrate. For thicker films the situation is different: the exchange process (Cu diffusing through the film) is necessarily slowed down and, as our data indicate, the primary channel

is the generation of pinholes from which Cu "flows" out to the surface. At still higher thickness (4–5 ML) even this channel is blocked, there are no pinholes generated, and, therefore there is no Cu appearing on the surface. The activation temperature for the nucleation of diffusion channels is surprisingly low – our estimation for 3 ML films ranges between 340 and 400 K. This agrees well with Auger data reported previously by Arnott et al. [35].

The driving force could be the interplay between the surface and interfacial free energies. The literature values [36,37] indicate $\sigma_{Cu} = 1.9$ J m^{-2}, $\sigma_{Fe} = 2.9$ J m^{-2} and $\sigma_{FeCu} = 0.6$ J m^{-2}. Thus, the total free energy of the system can be lowered either by Fe agglomeration or by forming a Cu–Fe–Cu sandwich. All our results consistently show that Fe agglomeration does not occur during annealing; one plausible explanation might be that the diffusion constants of Fe are smaller than those of Cu. As the driving force remains nearly the same as long as the thickness is below that required for fcc–bcc martensitic phase transformation [29], Cu will keep diffusing to the top of the surface until the system's free energy drops down to a certain value. Because the density of the pinholes decreases rapidly with increasing coverage, these holes tend to become wider and deeper in thicker films to make the same amount of Cu to diffuse to the top of the surface, as shown in Table 1. Kinetic limitations start to play a role at relatively low coverages around 4 ML – smaller pinhole density implies a longer distance Cu needs to migrate on the surface, so, as a consequence, the Fe–Cu surface alloy concentrates in the area around the holes (Fig. 3).

If the driving force for pinhole formation is really the surface free energy, then, simply capping the iron film with some amount of Cu should stop it. Indeed, when the iron film (3.5 ML) is capped by approximately 0.8 layer of Cu, and annealed for 10 min at 490 K the Auger ratios did not change, and, as shown in Fig. 12 no pinholes were formed. The Fe–Cu surface alloy corrugation patches do still appear on the surface just as expected. They look different from the Fe–Cu alloy in normally annealed Fe film, the reason might be due to the fact that they are in a different background (Cu and Fe respectively for Cu/Fe/Cu sandwich and Fe/Cu) or with a different composition. The result of this Cu capping experiment strongly indicates that the surface free energy is the only driving force for pinhole formation.

5. Conclusions

The results presented above show that the unusual diffusion mechanism observed for the first time in the Co/Cu(100) system is more general. Essentially identical behaviour is seen in Fe/Cu(100). This does not appear to be a coincidence. In both cases the balance of surface and interface energies favour formation of the sandwich structure and neither of the systems is miscible in bulk. Lack of miscibility prevents diffusion of substrate material to the surface through the film and the system can minimize its energy only by capping the surface with the material that flows out from microscopic channels to the substrate (pinholes, pits). These channels form only at elevated temperatures and their density depends on the thickness of the film.

At higher thicknesses, the dramatic reduction in nucleation density of pinholes may simply reflect the population density of some atomic imperfections (vacancies, impurities, dislocations, etc.) which serve as nucleation points for larger pinholes, or may simply reflect the energetic barrier for spontaneous creation of diffusion channels to the surface. High mobility of metallic adatoms makes vacancies an unlikely candidate for such sites even with the highly supersaturated iron vapour beam used in these experiments.

The second major finding reported here is the surface alloying that was not expected in a system which does not mix in the bulk. Microscopic intermixing (surface segregation) has been long established in this system as expected from surface tension data but extensive surface alloying is reported here for the first time. Its characteristic feature is the appearance of bias-dependent corrugation in STM images. Such a phase appears only at elevated temperatures even at submonolayer coverages, which is postulated to be due to enhanced clustering in the surface alloy.

In conclusion, we have systematically studied the annealing effect on the Fe/Cu(100) system by STM and AES. We would expect that similar behaviour

should be observed in systems where similar conditions (surface/interface energy balance, miscibility) exist like Cu/Ag, Pt/Au, etc.

Acknowledgements

We would like to thank J. Landgraf and G. Matalla for their helpful assistance with the STM experiments presented here.

References

[1] C.S. Wang, B.M. Klein and H. Krakauer, Phys. Rev. Lett. 54 (1985) 1852;
F.J. Pinski, J. Stautonton, B.L. Gyorffy, D.D. Johnson and G.M. Stocks, Phys. Rev. Lett. 56 (1986) 2096;
V.L. Moruzzi, P.M. Markus, K. Schwarz and P. Mohn, Phys. Rev. B 34 (1986) 1784.
[2] J.R. Dutcher, B. Heinrich, J.F. Cohran, D.A. Steigerwald and W.F. Egelhoff, Jr., J. Appl. Phys. 63 (1988) 3464.
[3] C. Liu, E.R. Moog and S.D. Bader, Phys. Rev. Lett. 60 (1988) 2422.
[4] D.P. Pappas, K.P. Kamper and H. Hopster, Phys. Rev. Lett. 64 (1990) 3179.
[5] R. Allenspach and A. Bischof, Phys. Rev. Lett. 69 (1992) 3385.
[6] J. Thomassen, F. May, B. Feldmann, M. Wuttig and H. Ibach, Phys. Rev. Lett. 69 (1992) 3831.
[7] P. Xhonneux and E. Courtens, Phys. Rev. B 46 (1992) 556.
[8] D.A. Steigerwald, I. Jacob and W.F. Egelhoff, Jr., Surf. Sci. 202 (1988) 472.
[9] M. Wuttig, B. Feldman, J. Thomassen, F. May, H. Zillgen, A. Brodde, H. Hannemann and H. Neddermeyer, Surf. Sci. 291 (1993) 14, and references therein.
[10] K.E. Johnson, D.D. Chambliss, R.J. Wilson and S. Chiang, J. Vac. Sci. Technol. A 11 (1993) 1654.
[11] W. Wiartolla, W. Becker, W. Keline and H.D. Pfannes, J. Phys. C 45 (1984) 461.
[12] M. Onellion, M.A. Thompson, J.L. Fu, J.L. Erskine and A.J. Freeman, Phys. Rev. B 33 (1986) 7322.
[13] R.C. Weast, M.J. Astle and W.H. Beyer, Eds., CRC Handbook of Chemistry and Physics (CRC Press, Boca Raton, FL, 1993).
[14] W.A. Macedo and W. Keune, Phys. Rev. Lett. 61 (1988) 475.
[15] D. Pescia, M. Stampanoni, G.L. Bona, A. Vaterlaus, F. Meier, G. Jennings and R.F. Willis, Phys. Rev. Lett. 60 (1988) 2559.
[16] J. Giergiel, J. Shen, J. Woltersdorf, A. Kirilyuk and J. Kirschner, submitted.
[17] E.R. Moog and S.D. Bader, Superlatt. Microstruct. 1 (1985) 543.
[18] K. Meinel, M. Klaua and H. Bethge, Ultramicroscopy 20 (1986) 261.
[19] W.F. Egelhoff, Jr., J. Vac. Sci. Technol. A 7 (1989) 2060.
[20] P.J. Schmitz et al., Phys. Rev. B 40 (1989) 11477.
[21] H. Li and B.P. Tonner, Surf. Sci. 237 (1990) 141.
[22] T. Detzel and N. Memmel, Phys. Rev. B 49 (1994) 5599.
[23] A.K. Schmid, D. Atlan, H. Itoh, B. Heinrich, T. Ichinokawa and J. Kirschner, Phys. Rev. B 48 (1993) 2855.
[24] A.K. Schmid, PhD Thesis, FU Berlin, 1992.
[25] A.K. Schmid and J. Kirschner, J. Vac. Sci. Technol. B 9 (1991) 649.
[26] This STM is run by NanoScope III software (version 2.53); film coverages were calculated with the histogram function of this software.
[27] K.E. Johnson, D.D. Chambliss, R.J. Wilson and S. Chiang, Surf. Sci. 313 (1994) L811.
[28] W.B. Pearson, A Handbook of Lattice Spacing and Structures of Metals and Alloys (Pergamon, New York, 1958).
[29] J. Giergiel, J. Kirschner, J. Landgraf, J. Shen and J. Woltersdorf, Surf. Sci. 310 (1994) 1.
[30] D.D. Chambliss, R.J. Wilson and S. Chiang, J. Vac. Sci. Technol. A 10 (1992) 1993.
[31] F. Besenbacher and I. Stensgaard, in: The Chemical Physics of Solid Surfaces and Heterogeneous Catalysis, Eds. D.A. King and D.P. Woodruff (Elsevier, Amsterdam, 1993) ch. 15.
[32] M. Schmid, H. Stadler and P. Varga, Phys. Rev. Lett. 70 (1993) 1441.
[33] A. Zangwill, Physics at Surfaces (Cambridge University Press, Cambridge, 1988).
[34] Y.W. Mo and F.J. Himpsel, Phys. Rev. B 50 (1994) 7868.
[35] M. Arnott, E.M. McCash and W. Allison, Surf. Sci. 269/270 (1992) 724.
[36] L.Z. Mezey and J. Giber, Jpn. J. Appl. Phys. 21 (1982) 1569.
[37] W.A. Jesser and J.W. Matthews, Philos. Mag. 17 (1968) 595.